Title

Bias correction of gauge-based gridded product to improve extreme precipitation analysis in the Yarlung Tsangpo-Brahmaputra River basin

Author names and affiliations

Xian Luo[1,2], Xuemei Fan[1], Yungang Li[1,2], and Xuan Ji[1,2]

[1]Institute of International Rivers and Eco-security, Yunnan University, Kunming, China

[2]Yunnan Key Laboratory of International Rivers and Transboundary Eco-security, Kunming, China

Address

Institute of International Rivers and Eco-security, Yunnan University,

South Section, East Outer Ring Road, Chenggong District, Kunming, China

Email

Xian Luo: luoxian@ynu.edu.cn

Xuemei Fan: fanxuemei7@163.com

Yungang Li: ygli@ynu.edu.cn

Xuan Ji: jixuan@ynu.edu.cn

Contact Author: Xian Luo (luoxian@ynu.edu.cn)

Second Contact Author: Yungang Li (ygli@ynu.edu.cn)

Abstract. Critical gaps in the amount, quality, consistency, availability, and spatial distribution of rainfall data limit extreme precipitation analysis, and the application of gridded precipitation data are challenging because of their considerable biases. This study corrected Asian Precipitation Highly Resolved Observational Data Integration Towards Evaluation of Water Resources (APHRODITE) estimates in the Yarlung Tsangpo-Brahmaputra River basin (YBRB) using two linear and two nonlinear methods, and their influence on extreme precipitation indices were assessed by cross-validation. Bias correction greatly improved the performance of extreme precipitation analysis. The ability of four methods to correct wet-day frequency and coefficient of variation were substantially different, leading to considerable differences in extreme precipitation indices. Local intensity scaling (LOCI) and quantile−quantile mapping (QM) performed better than linear scaling (LS) and power transformation (PT). This study would provide reference for using gridded precipitation data in extreme precipitation analysis and selecting bias-corrected method for rainfall products in data-sparse regions.

1 Introduction

Extreme precipitation often leads to floods, debris flows, and other secondary disasters (Wang et al., 2017), and changes in the frequency and intensity of extreme precipitation profoundly influence both natural environment and human society profoundly (Easterling et al., 2000; Yucel and Onen, 2014). Rainfall observations provide a primary foundation for comprehending their long-term variability and change in extreme precipitation (Alexander, 2016). Accurate rainfall data are necessary for flood protection and water resource management. However, due to scarce spatial coverage of rainfall stations, short-length rainfall records, and high proportions of missing data,

observations currently available in some remote basins are clearly inadequate to capture their precipitation characteristics. In addition, observed rainfall data are usually difficult to collect in international river basins because many countries may not share or freely distribute data (Lakshmi et al., 2018).

The Yarlung Tsangpo-Brahmaputra River is the fourth largest river in the world in terms of flow (Kamal-Heikman et al., 2007), which is influenced profoundly by complex atmospheric dynamics and regional climate processes (Immerzeel et al., 2010; Pervez and Henebry, 2015). Because its agriculture and economy rely heavily on monsoon precipitation, the basin is particularly vulnerable to changing climate (Singh et al., 2016; Liu et al., 2018; Janes et al., 2019; Xu et al., 2019; Zhang et al., 2019). During the four summer monsoon months of June, July, August, and September (JJAS), extreme precipitation with large uncertainties lead to numerous floods (Kamal-Heikman et al., 2007; Dimri et al., 2016; Malik et al., 2016). However, the understanding on extreme precipitation in the Yarlung Tsangpo-Brahmaputra River basin (YBRB) have a number of gaps because of its complex topographic interactions with atmospheric flows, lack of observations, and data sharing issues, which hinder effective flood management (Ray et al., 2015; Prakash et al., 2019).

Currently, different gridded rainfall products provide effective information over regional to global scales, which could be broadly classified into four categories: (1) gauge-based data sets that build on observations from rainfall stations; (2) products from numerical weather predictions or atmospheric models; (3) satellite-only products; and (4) combined satellite-gauge products. The performance of these products vary from region to region (Duan et al., 2016). Given the heterogeneity of orography and climate in the YBRB, observing and modeling its precipitation are very challenging (Khandu et al., 2017). In addition, satellite products are less reliable because high

67 convective rainfall generally takes place in the southern foothills of the Himalayas (Prakash et al.,
68 2015). Compared with some other gauge-based products, Asian Precipitation Highly Resolved
69 Observational Data Integration Towards Evaluation of Water Resources (APHRODITE) dataset
70 collected more rainfall observations across South Asia (Rana et al., 2015), which have been proved
71 could better estimate spatial precipitation (Andermann et al., 2011). Nonetheless, the lack and
72 uneven distribution of rainfall stations at high altitudes in the Tibetan Plateau and Himalayas may
73 introduce uncertainty and affect the accuracy of APHRODITE estimates (Rana et al., 2015;
74 Chaudhary et al., 2017).

75 Numerous rainfall observations can be obtained from public databases, although their short
76 record and static character limit their direct application in precipitation analysis (Donat et al., 2013).
77 However, these data could be useful for bias correction of gauge-based gridded products by
78 providing additional observations from the denser network of rainfall stations. On the other hand,
79 ranging from simple linear scaling to more sophisticated nonlinear approaches, several methods
80 have been developed to adjust global climate model (GCM) data (Teutschbein and Seibert, 2012).
81 Similarly, these bias correction methods could be applied to correct gridded rainfall products in
82 sparsely-gauged mountainous basins (He et al., 2017). It is important to study whether extreme
83 precipitation analysis could be improved by bias correction of gridded precipitation data and how
84 different methods would influence extreme precipitation indices.

85 This study evaluated different bias correction approaches for APHRODITE estimates in the
86 YBRB and assessed their effects on extreme precipitation analysis. We first corrected APHRODITE
87 estimates by both linear and nonlinear methods. Next, we calculated extreme precipitation indices
88 using original and different corrected APHRODITE estimates, and the effects of bias correction on

extreme precipitation analysis were further investigated by cross-validation. The results would support reference for the application of gridded precipitation data and bias-corrected methods in extreme precipitation analysis.

2 Material and methods

2.1 Study area

The YBRB can be divided into three physiographic zones: (1) the Tibetan plateau (TP), covering 44.4% of the basin, with elevations above 3500 m; (2) the Himalayan belt (HB), accounting for 28.6% of the basin, with elevations ranging from 100 m to 3500 m; and (3) the floodplains (FP), covering 27.0% of the basin, with elevations up to 100 m (Immerzeel, 2008).

The moisture in the YBRB is mainly from the Indian Ocean. The YBRB exhibits a broad range of precipitation from the semi-arid upstream areas to the HB characterized by abundant orographic rainfall as well as the vast humid FP. In the upstream areas, precipitation is concentrated during JJAS, and rainfall intensity is mostly low due to long-distance moisture transport (Guan et al., 1984). The irregular topographic variations in the Himalayas profoundly affect the spatial distribution of precipitation by altering monsoonal flow, producing intense orographic rainfall along the Himalayan foothills (Khandu et al., 2017). The downstream areas also receive high rainfall from monsoon flow during JJAS, accounting for 60%−70% of the annual rainfall (Gain et al., 2011).

2.2 Data sources

2.2.1 Observational data

In the upper YBRB, rainfall data across China recorded at 31 meteorological stations were

collected from the National Meteorological Information Center (NMIC, sourced from the China Meteorological Data Sharing Service System). In addition, data observed at 91 rainfall stations in the downstream area were obtained from the Global Historical Climatology Network (GHCN)−Daily dataset for bias correction. GHCN-Daily dataset comprises observations from four sources, which have been undergone extensive quality reviews, including the U.S. Collection, the International Collection, the Government Exchange Data, and the Global Summary of the Day. The locations of rainfall stations are shown in Fig. 1.

2.2.2 APHRODITE estimates

Numerous rainfall observations were incorporated into APHRODITE estimates, including (1) Global Telecommunication System (GTS)-based data, (2) data obtained from other projects or organizations, and (3) their own collection. The rainfall observations that had undergone quality control were gathered, and the ratios of rainfall observations to the world climatology were calculated and then interpolated for each month. The interpolated ratios were multiplied by the world climatology, and the first six components of the fast Fourier transform of the resulting values were used to obtain daily precipitation (Yatagai et al., 2012).

Daily rainfall data of APHRO_MA_025deg_V1101 (http://aphrodite.st.hirosaki-u.ac.jp/index.html) at 0.25° resolution in the Asian monsoon area end in 2007, while recently published APHRO_MA_025deg_V1101EX_R1 (http://aphrodite.st.hirosaki-u.ac.jp/index.html), using the same algorithm and spatial resolution, extend the time series over the period 2007−2015. Therefore, extreme precipitation could be analyzed during 1951−2015 by applying both datasets. To investigate the influence of topography on bias-corrected APHRODITE estimates, the grids were

133 classified into three topographic zones (the TP, HB, and FP; Fig. 2).

134

135 **2.3 Methods**

136 **2.3.1 Bias correction methods**

137 Two linear methods (linear scaling (LS) and local intensity scaling (LOCI)) and two non-linear
138 methods (power transformation (PT) and quantile−quantile mapping (QM)) were used for bias
139 correction in this study.

140 (1) LS

141 LS corrects monthly estimates in accordance with observations (Lenderink et al., 2007). It
142 corrects APHRODITE estimates using the ratio between mean monthly observation and
143 corresponding estimation:

144 $$P^{*}_{APH}(d) = P_{APH}(d) \cdot \left[\frac{\mu_m\left(P_{obs}(d)\right)}{\mu_m\left(P_{APH}(d)\right)} \right] \quad (1)$$

145 where $P^{*}_{APH}(d)$ and $P_{APH}(d)$ are the daily precipitation of corrected and original APHRODITE
146 estimate, respectively, and $P_{obs}(d)$ is the daily precipitation observed at the rainfall station in
147 corresponding grid of the APHRODITE estimate. $\mu_m\left(P_{obs}(d)\right)$ and $\mu_m\left(P_{APH}(d)\right)$ are the mean
148 monthly precipitation of observations and corresponding APHRODITE estimates in the *m*th month,
149 respectively.

150 (2) LOCI

151 LOCI makes a flexible adjustment to the wet-day frequency and intensity (Schmidli et al., 2006;
152 Teutschbein and Seibert, 2012). Firstly, an adjusted precipitation threshold ($P_{th,APH}$) is determined so
153 that the number of days exceeding this threshold for APHRODITE estimates matches that of
154 observed days with precipitation larger than 0 mm. Secondly, a linear scaling factor (*s*) for wet days

155 is computed:

156 $$s = \frac{\mu_m\left(P_{obs}(d)\middle|P_{obs}(d) > 0 \text{ mm}\right)}{\mu_m\left(P_{APH}(d)\middle|P_{APH}(d) > P_{th,APH}\right) - P_{th,APH}} \quad (2)$$

157 where $\mu_m\left(P_{obs}(d)\middle|P_{obs}(d) > 0 \text{ mm}\right)$ is the mean monthly precipitation of observations with daily

158 precipitation larger than 0 mm, and $\mu_m\left(P_{APH}(d)\middle|P_{APH}(d) > P_{th,APH}\right)$ is the mean monthly precipitation

159 of APHRODITE estimates with daily precipitation larger than $P_{th,APH}$. Finally, the precipitation data

160 are corrected, using:

161 $$P^*_{APH}(d) = \max\left(s \cdot \left(P_{APH}(d) - P_{th,APH}\right), 0\right) \quad (3)$$

162 (3) PT

163 PT corrects both the mean and the coefficient of variation of precipitation (Leander and

164 Buishand, 2007), changing precipitation by:

165 $$P^*_{APH}(d) = a \cdot \left(P_{APH}(d)\right)^b \quad (4)$$

166 where *a* and *b* are the parameters of the power transformation, which are obtained using a

167 distribution-free approach and estimated for each month within a 90-day window. Using a root-

168 finding algorithm, the value of *b* is firstly determined to ensure that the coefficient of variation of

169 the corrected estimates matches that of the observations. The parameter *a* is then calculated using

170 the mean observation and the corresponding mean of the transformed values.

171 (4) QM

172 By shifting occurrence distributions, QM corrects the distribution function of precipitation

173 estimates to match that of observations, which is commonly used in correcting systematic

174 distributional biases (Cannon et al., 2015). A Gamma distribution is usually assumed for

175 precipitation events (Teutschbein and Seibert, 2012):

$$f_\gamma\left(x|\alpha,\beta\right)=x^{\alpha-1}\cdot\frac{1}{\beta^\alpha\cdot\Gamma\left(\alpha\right)}\cdot e^{-\frac{x}{\beta}};x\geq 0;\alpha,\beta>0 \quad (5)$$

where α and β are the shape parameter and scale parameter, respectively.

The cumulative density function (CDF) of the APHRODITE estimates is adjusted to agree with that of the observation, and the daily precipitation for APHRODITE estimates is corrected depending on its quantile. It should be noted that for APHRODITE estimates, many days had low precipitation estimates instead of substantial dry conditions, which may distort the distribution of daily precipitation. Therefore, an adjusted precipitation threshold is also used to ensure the wet-day frequency of corrected APHRODITE estimates match the observed frequency:

$$P_{APH}^{*}\left(d\right)=\begin{cases}0, & \text{if} \quad P_{APH}\left(d\right)<P_{th,APH}\\ F_\gamma^{-1}\left(F_\gamma\left(P_{APH}\left(d\right)|\alpha_{APH,m},\beta_{APH,m}\right)|\alpha_{obs,m},\beta_{obs,m}\right), & \text{otherwise}\end{cases} \quad (6)$$

F_γ and F_γ^{-1} are the Gamma CDF and its inverse, respectively. $\alpha_{APH,m}$ and $\beta_{APH,m}$ are the shape parameter and scale parameter of original APHRODITE estimates in the *m*th month, respectively, and $\alpha_{obs,m}$ and $\beta_{obs,m}$ are those of observations in the *m*th month, respectively.

This study corrected the grids of the APHRODITE estimates that contained time series of observations, and the parameters of bias correction were determined using corresponding available rainfall observations. After that, the APHRODITE estimates during 1951−2015 in these grids were corrected by four bias correction methods, respectively. Hereafter, APHRODITE estimates corrected by LS, LOCI, PT, and QM are referred as LS-APHRODITE, LOCI-APHRODITE, PT-APHRODITE, and QM-APHRODITE estimates, respectively.

2.3.2 Indices of extreme precipitation

To characterize extreme precipitation during JJAS, six indices recommended by the Expert Team on Climate Change Detection and Indices (ETCCDI), including consecutive wet days (CWD),

number of heavy precipitation days (R10mm), number of very heavy precipitation days (R20mm), maximum 1-day precipitation amount (Rx1d), maximum 5-day precipitation amount (Rx5d), and simple daily intensity index (SDII), were applied in this study. Detailed descriptions of these indices are shown in Table 1. The indices fall roughly into three categories: (1) duration indices, which represent the length of the wet spell; (2) threshold indices, which count the days on which a fixed precipitation threshold is exceeded; (3) absolute indices, which describe the maximum 1-day or 5-day precipitation amount (Sillmann et al., 2013).

Extreme precipitation indices for corrected APHRODITE estimates in the grids distributed with rainfall stations were calculated. To obtain extreme precipitation indices in other grids, inverse distance weighted (IDW) interpolation for extreme precipitation indices were performed. This allowed us to calculate mean values for each of the three topographic zones.

2.3.3 Validation on bias correction

Cross-validation was applied to evaluate the performance of four bias correction methods. At each rainfall station, the observations were divided into two groups. Two-thirds of the rainfall records were applied to calculate the parameters of LS, LOCI, PT, and QM, respectively. Making use of these parameters, the APHRODITE estimates were then corrected. The mean error (*ME*) between the extreme precipitation indices obtained from the corrected APHRODITE estimates and those obtained from remaining one-third of the rainfall observations were calculated to evaluate the performance of different bias correction methods.

3 Results

3.1 Evaluation of extreme precipitation indices

The *ME* of extreme precipitation indices during JJAS for validation are shown in Fig. 3. For original APHRODITE estimates, the *ME* of CWD in the TP, HB, and FP were 8.3, 16.4, and 21.8 days, respectively. There were a lot of days with low precipitation estimations instead of substantial dry conditions, leading to the overestimation on CWD. Likewise, this propagated to LS-APHRODITE estimates with similar *ME* of CWD, because there was no change made to the wet-day frequency. The *ME* of CWD in the TP, HB, and FP for LOCI-APHRODITE estimates were 3.1, 1.2, and 1.4 days, respectively, and those for QM-APHRODITE estimates were 2.5, 0.8, and 0.9 days, respectively. For both LOCI- and QM-APHRODITE estimates, the days with low precipitation estimations instead of substantial dry conditions were redefined as dry days using precipitation threshold, resulting in much less *ME* and more reliable CWD. Finally, although PT did not directly correct wet-day frequency, the CWD for PT-APHRODITE estimates were lower than those for original APHRODITE estimates because tiny precipitation were corrected.

Original APHRODITE tended to underestimate heavy and very heavy precipitation days. Bias correction reduced error on R10mm and R20mm except LS, and the absolute value of mean *ME* for LOCI-, PT-, and QM-APHRODITE estimates were mostly less than 1.0 days. LOCI, PT, and QM are able to effectively correct heavy and very heavy precipitation days.

For original APHRODITE estimates, the *ME* of Rx1d were −11.3, −89.1 and −50.5 mm in the TP, HB, and FP, respectively, and those of Rx5d reached −18.0, −167.4 and −76.8 mm, respectively. Original APHRODITE estimates greatly underestimated Rx1d and Rx5d. For corrected APHRODITE estimates, QM performed best on Rx1d, and the *ME* for QM-APHRODITE estimates were −0.1, −1.9 and −5.4 mm, respectively. LS and LOCI used consistent ratio in linear

242 transformation, resulting in underestimation on Rx1d. In addition, LOCI outperformed other
243 methods on Rx5d, and the overestimation in the HB and FP for PT- and QM-APHRODITE estimates
244 were greater.

245 The *ME* of SDII for original APHRODITE estimates in the TP, HB, and FP were −2.4, −13.9
246 and −11.0 mm, respectively. Firstly, heavy and very heavy precipitation in the HB and TP were not
247 fully captured by original APHRODITE estimates. Secondly, original APHRODITE estimates
248 overestimated wet days, which distorted the estimation of precipitation intensity. Smaller error were
249 found in LOCI- and QM-APHRODITE estimates because they corrected rainfall amount as well as
250 the number of rainy days.

251

252 **3.2 Extreme precipitation indices calculated from original and corrected APHRODITE**
253 **estimates**

254 **3.2.1 Extreme precipitation indices in the three physiographic zones**

255 Extreme precipitation indices calculated from original and four corrected APHRODITE
256 estimates in the three different physiographic zones are shown in Fig. 4. The CWD estimated using
257 original APHRODITE and LS-APHRODITE estimates were similar. Meanwhile, those derived
258 from LOCI-, PT-, and QM-APHRODITE estimates were much less.

259 Mean R10mm during JJAS obtained by original APHRODITE estimates in the TP, HB, and FP
260 were 6.7, 31.0, and 47.7 days, respectively. These were similar to those estimated by corrected
261 APHRODITE estimates. However, the differences in R20mm were much pronounced. Mean
262 R20mm in HB and FP for bias-corrected APHRODITE datasets were close to 19.0 and 26.5 days,
263 respectively, which were approximately 4–5 days higher than those derived from original

APHRODITE estimates.

Compared with original APHRODITE estimates, the Rx1d and Rx5d increased greatly after bias correction. In the HB, the mean Rx1d obtained from original APHRODITE estimates was 49.5 mm, while those for LS-, LOCI-, PT-, and QM-APHRODITE estimates were 72.4, 90.1, 109.0, and 103.8 mm, respectively. In addition, the ranges of Rx1d and Rx5d also increased considerably.

The differences in SDII between original and corrected APHRODITE estimates were also marked. For example, mean SDII in the FP calculated from original APHRODITE estimates was 13.4 mm. After correction, mean SDII for LOCI- and QM-APHRODITE estimates increased to 23.4 and 25.1 mm, respectively. These values were much greater than those derived from LS- and PT-APHRODITE datasets (15.7 and 17.7 mm).

3.2.2 Relative changes in extreme precipitation indices

The relative changes in extreme precipitation indices during JJAS based on original and corrected APHRODITE estimates are shown in Fig. 5. The CWD for LOCI-, PT-, and QM-APHRODITE estimates were all lower than original APHRODITE estimates, yielding relative change rates from −66% to −27%. Bias correction decreased the number of rainy days except LS. The variations in R10mm and R20mm illustrated that corrected APHRODITE estimates identified much more extreme precipitation events in the TP. The changes in indices varied considerably for different correction methods, with the change rates of R20mm in the TP for LS-, LOCI-, PT-, and QM-APHRODITE estimates being 30.4%, 169.2%, 297.1%, and 317.4%, respectively. For Rx1d, Rx5d, and SDII, the increases in the HB were much pronounced than those in the FP and TP. Except for LS-APHRODITE estimates, the increases in Rx1d and Rx5d in the HB were all above 70% for

corrected APHRODITE estimates.

3.3 Influence of bias correction on the spatial distribution of extreme precipitation indices

Rainstorms over the lower YBRB usually have the duration of 2−3 days (Dhar and Nandargi, 2000), and large multi-day precipitation events are crucial to the floods in the basin. Hence, the spatial distribution of Rx5d during JJAS based on original APHRODITE estimates were compared with corrected APHRODITE estimates in Fig. 6. For original APHRODITE estimates, the area with Rx5d higher than 300 mm only accounted for 2.0% of the basin, while the proportions for LS-, LOCI-, PT-, and QM-APHRODITE estimates were 10.9%, 18.7%, 21.7%, and 21.3%, respectively. The most profound difference between original and corrected APHRODITE estimates occurred over the windward slopes of the Himalayas before the river flows into the Brahmaputra valley. The Rx5d calculated from original APHRODITE estimates were lower than 300 mm, while much higher Rx5d were obtained after bias correction, yielding maxima of 946.6, 1030.3, 1105.1, and 1396.6 mm for LS-, LOCI-, PT-, and QM-APHRODITE estimates, respectively. The eastern Himalayas, acting as orographic barriers, push the southwest moist air upwards, leading to heavier extreme precipitation over the windward slopes (Singh et al., 2004; Bookhagen and Burbank, 2010; Dimri et al., 2016). However, original APHRODITE estimates tended to substantially underestimate these extreme precipitation. Besides aforementioned region, higher Rx5d along the Himalayan front were also found after bias correction. In this case, extreme precipitation calculated from nonlinear approaches were heavier than those derived from linear methods. In general, bias correction are able to consider topographic effects on the spatial distribution of extreme precipitation more comprehensively.

4 Discussion

Using two linear and two nonlinear bias methods, we corrected APHRODITE estimates during JJAS in the YBRB to investigate the effects of different approaches on extreme precipitation analysis. Extreme precipitation indices were strongly dependent on the bias correction approach applied.

A primary problem when using gauge-based gridded data sets for extreme precipitation analysis is the fundamental mismatch between point-based observations and gridded estimates (Alexander, 2016). In addition, the spatial coverage of rainfall stations is another major source of uncertainty, particularly where spatial distributions of precipitation are complex (Donat et al., 2013). There are currently several approaches for bias correction, ranging from simple linear scaling to more sophisticated nonlinear methods (Teutschbein and Seibert, 2012). Although mean precipitation corrected by all bias-corrected approaches were similar, their standard deviations and consequent extreme precipitation indices varied considerably. In the case of linear correction, both mean and standard deviation are multiplied by same factor (Leander and Buishand, 2007), resulting in dubious variations of precipitation. Nonlinear correction adjust mean and also coefficient of variation (Teutschbein and Seibert, 2012), yielding more reliable results. In addition, the typical biases of rainfall products are related to their identification of too many wet days with low-intensity precipitation. Among the four bias-corrected approaches applied herein, LS and PT make no change on the number of rainy days, while LOCI and QM use threshold exceedance to match the wet-day frequency to the observations.

In international river basins, rainfall data are usually not publicly available, and extreme precipitation analysis may suffer from data restrictions (Nishat and Rahman, 2009; Luo et al., 2019).

Several great international rivers in south Asia, including the Indus, Ganges, and Yarlung Tsangpo−Brahmaputra, originate from or flow through the Himalayas. Topographic variations of the Himalayas profoundly influence the spatial distribution of precipitation by altering monsoonal flow, resulting in considerable orographic rainfall on the windward slopes (Khandu et al., 2017). Rainfall estimates of different products varied markedly along the Himalayan front and obtained similar results toward the adjacent low-relief domains (Andermann et al., 2011). The GHCN-Daily data can be applied to correct gauge-based gridded data sets in this region, ensuring these products capture the spatial distribution and variation of extreme precipitation. However, numerous GHCN-Daily records in Asia do not contain data from recent years, and the short or incomplete rainfall records limit their direct applications (Donat et al., 2013). Hence, it would be preferable to apply nonpublic datasets in data-sparse regions.

5 Conclusions

Despite increasing use of gridded rainfall products in sparsely gauged river basins, their application in extreme precipitation analysis is challenging due to considerable biases. This study made use of four methods to correct APHRODITE estimates in the YBRB. Their influences on extreme precipitation indices were compared and assessed. The following conclusions were drawn.

(1) Original APHRODITE estimates tended to underestimate heavy and very heavy precipitation in the YBRB, and there were a lot of days with low precipitation estimations instead of substantial dry conditions. Bias correction greatly improved the performance of extreme precipitation analysis. The extreme precipitation indices calculated from different corrected APHRODITE estimates varied substantially, and LOCI- and QM-APHRODITE estimates were able

to obtain more reliable extreme precipitation indices.

(2) Insufficient gauge observations in the Himalayas caused high uncertainty in the heavy precipitation estimates for original APHRODITE estimates. After bias correction using observations from a denser network of gauges, the heterogeneous orographic effects on extreme precipitation were captured more accurately.

Data availability. The co-authors used publicly available data from the Asian Precipitation Highly Resolved Observational Data Integration Towards Evaluation of Water Resources and the National Centers for Environmental Information. In addition, rainfall observations in China were obtained from the National Meteorological Information Center.

Author contributions. XL and YL conceived the study, XL and XF carried out bias correction and extreme precipitation analysis, XL drafted the paper, and all co-authors jointly worked on enriching and developing the draft.

Competing interests. The authors declare that they have no conflict of interest.

Acknowledgements. This study was supported by the National Natural Science Foundation of China (41661144044, 41601026), the National Key R&D Program of China (2016YFA0601601), and the Science and Technology Planning Project of Yunnan Province, China (2017FB073).

References

374 Alexander, L. V.: Global observed long-term changes in temperature and precipitation extremes: A
375 review of progress and limitations in IPCC assessments and beyond, Weather & Climate Extremes,
376 11, 4–16, https://doi.org/10.1016/j.wace.2015.10.007, 2016.
377 Andermann, C., Bonnet, S., and Gloaguen, R.: Evaluation of precipitation data sets along the
378 Himalayan front, Geochemistry, Geophysics, Geosystems, 12, Q07023,
379 https://doi.org/10.1029/2011gc003513, 2011.
380 Bookhagen, B. and Burbank, D. W.: Toward a complete Himalayan hydrological budget:
381 Spatiotemporal distribution of snowmelt and rainfall and their impact on river discharge, Journal of
382 Geophysical Research, 115, F03019, https://doi.org/doi:10.1029/2009JF001426, 2010.
383 Cannon A. J., Sobie S. R., and Murdock T. Q.: Bias correction of GCM precipitation by quantile
384 mapping: How well do methods preserve changes in quantiles and extremes? Journal of Climate,
385 28, 6938–6959, https://doi.org/10.1175/JCLI-D-14-00754.1, 2015.
386 Chaudhary S., Dhanya C. T., and Vinnarasi R.: Dry and wet spell variability during monsoon in
387 gauge-based gridded daily precipitation datasets over India, Journal of Hydrology, 546, 204–218,
388 https://doi.org/10.1016/j.jhydrol.2017.01.023, 2017.
389 Dhar, O. N. and Nandargi, S.: A study of floods in the Brahmaputra Basin in India, International
390 Journal of Climatology, 20, 771–781, 2000.
391 Dimri, A. P., Thayyen, R. J., Kibler, K., Stanton, A., Jain, S. K., Tullos, D., and Singh, V. P.: A review
392 of atmospheric and land surface processes with emphasis on flood generation in the Southern
393 Himalayan rivers, Science of the Total Environment, 556, 98 – 115,
394 http://dx.doi.org/10.1016/j.scitotenv.2016.02.206, 2016.
395 Donat, M. G., Alexander, L. V., Yang, H., Durre, I., Vose, R., and Caesar, J.: Global land-based

396 datasets for monitoring climatic extremes, Bulletin of the American Meteorological Society, 94,
397 997–1006, http://dx.doi.org/10.1175/BAMS-D-12-00109.1, 2013.
398 Duan, Z., Liu, J., Tuo, Y., Chiogna, G., and Disse, M.: Evaluation of eight high spatial resolution
399 gridded precipitation products in Adige Basin (Italy) at multiple temporal and spatial scales, Science
400 of the Total Environment, 573, 1536–1553, http://dx.doi.org/10.1016/j.scitotenv.2016.08.213, 2016.
401 Easterling, D. R.: Climate extremes: observations, modeling, and impacts, Science, 289, 2068–2074,
402 https://doi.org/doi:10.1126/science.289.5487.2068, 2000.
403 Gain, A. K., Immerzeel, W. W., Sperna Weiland, F. C., and Bierkens, M. F. P.: Impact of climate
404 change on the stream flow of the lower Brahmaputra: trends in high and low flows based on
405 discharge-weighted ensemble modelling, Hydrology and Earth System Sciences, 15, 1537–1545,
406 https://doi.org/10.5194/hess-15-1537-2011, 2011.
407 Guan, Z. H., Chen, C. Y., Ou, Y. X., Fan, Y. Q., Zhang, Y. S., Chen, Z. M., Bao, S. H., Zu, Y. T., He,
408 X. W., and Zhang, M. T. (Eds.): Rivers and Lakes in Tibet, Science Press, Beijing, China, 1984.
409 He, Z., Hu, H., Tian F., Ni G., and Hu Q.: Correcting the TRMM rainfall product for hydrological
410 modelling in sparsely-gauged mountainous basins, Hydrological Sciences Journal, 62, 306–318,
411 https://doi.org/10.1080/02626667.2016.1222532, 2017.
412 Immerzeel, W.: Historical trends and future predictions of climate variability in the Brahmaputra
413 basin, International Journal of Climatology, 28, 243−254, https://doi.org/10.1002/joc.1528, 2008.
414 Immerzeel, W. W., van Beek, L. P. H., and Bierkens, M. F. P.: Climate change will affect the Asian
415 water towers, Science, 328, 1382−1385, https://doi.org/10.1126/science.1183188, 2010.
416 Janes, T., Mcgrath, F., Macadam, I., and Jones, R.: High-resolution climate projections for south
417 Asia to inform climate impacts and adaptation studies in the Ganges-Brahmaputra-Meghna and

418 Mahanadi deltas, Science of The Total Environment, 650, 1499 – 1520,
419 https://doi.org/10.1016/j.scitotenv.2018.08.376, 2019.
420 Kamal-Heikman, S., Derry, L. A., Stedinger, J. R., and Duncan, C. C.: A simple predictive tool for
421 lower Brahmaputra River basin monsoon flooding, Earth Interactions, 11, 1 – 11,
422 https://doi.org/10.1175/EI226.1, 2007.
423 Khandu, Awange, J. L., Kuhn, M., Anyah, R., and Forootan, E.: Changes and variability of
424 precipitation and temperature in the Ganges-Brahmaputra-Meghna River Basin based on global
425 high-resolution reanalyses, International Journal of Climatology, 37, 2141−2159,
426 https://doi.org/10.1002/joc.4842, 2017.
427 Lakshmi, V., Fayne, J., and Bolten, J.: A comparative study of available water in the major river
428 basins of the world, Journal of Hydrology, 567, 510 – 532,
429 https://doi.org/10.1016/j.jhydrol.2018.10.038, 2018.
430 Leander, R. and Buishand, T. A.: Resampling of regional climate model output for the simulation of
431 extreme river flows, Journal of Hydrology, 332, 487 – 496,
432 https://doi.org/10.1016/j.jhydrol.2006.08.006, 2007.
433 Lenderink, G., Buishand, A., and van Deursen, W.: Estimates of future discharges of the river Rhine
434 using two scenario methodologies: direct versus delta approach, Hydrology and Earth System
435 Sciences, 11, 1145–1159, https://doi.org/10.5194/hess-11-1145-2007, 2007.
436 Liu, Z., Wang, R., and Yao, Z.: Climate change and its impact on water availability of large
437 international rivers over the mainland Southeast Asia, Hydrological Processes, 32, 3966−3977,
438 https://doi.org/10.1002/hyp.13304, 2018.
439 Luo, X., Wu, W., He, D., Li, Y., and Ji, X.: Hydrological simulation using TRMM and CHIRPS

precipitation estimates in the lower Lancang-Mekong River Basin, Chinese Geographical Science, 29, 13–25, https://doi.org/10.1007/s11769-019-1014-6, 2019.

Malik, N., Bookhagen, B., and Mucha, P. J.: Spatiotemporal patterns and trends of Indian monsoonal rainfall extremes, Geophysical Research Letters, 43, 1710, https://doi.org/doi:10.1002/2016GL067841, 2016.

Nishat, B. and Rahman, S. M. M.: Water resources modeling of the Ganges-Brahmaputra-Meghna River basins using satellite remote sensing data, Journal of the American Water Resources Association, 45, 1313−1327, https://doi.org/10.1111／j.1752-1688.2009.00374.x, 2009.

Pervez, M. S. and Henebry, G. M.: Spatial and seasonal responses of precipitation in the Ganges and Brahmaputra river basins to ENSO and Indian Ocean dipole modes: implications for flooding and drought, Nat. Hazards Earth Syst. Sci., 15, 147–162, https://doi.org/10.5194/nhess-15-147-2015, 2015.

Prakash, S., Mitra, A. K., Momin, I. M., Rajagopal, E. N., Basu, S., Collins, M., Turner, A. G., Rao, K. A., and Ashok, K.: Seasonal intercomparison of observational rainfall datasets over India during the southwest monsoon season, International Journal of Climatology, 35, 2326−2338, https://doi.org/10.1002/joc.4129, 2015.

Prakash, S., Seshadri, A., Srinivasan, J., and Pai, D. S.: A new parameter to assess impact of rain gauge density on uncertainty in the estimate of monthly rainfall over India, Journal of Hydrometeorology, 20, 821–832, https://doi.org/10.1175/JHM-D-18-0161.1, 2019.

Rana, S., McGregor, J., and Renwick, J.: Precipitation seasonality over the Indian subcontinent: an evaluation of gauge, reanalyses, and satellite retrievals, Journal of Hydrometeorology, 16, 631−651, https://doi.org/10.1175/jhm-d-14-0106.1, 2015.

462 Ray, P. A., Yang, Y. E., Wi, S., Khalil, A., Chatikavanij, V., and Brown, C.: Room for improvement:
463 Hydroclimatic challenges to poverty-reducing development of the Brahmaputra River basin,
464 Environmental Science & Policy, 54, 64−80, https://doi.org/10.1016/j.envsci.2015.06.015, 2015.
465 Schmidli, J., Frei, C., and Vidale, P. L.: Downscaling from GCM precipitation: a benchmark for
466 dynamical and statistical downscaling methods, International Journal of Climatology, 26, 679–689,
467 https://doi.org/10.1002/joc.1287, 2006.
468 Sillmann, J., Kharin, V. V., Zhang, X., Zwiers, F. W., and Bronaugh, D.: Climate extremes indices
469 in the CMIP5 multimodel ensemble: Part 1. Model evaluation in the present climate, Journal of
470 Geophysical Research: Atmospheres, 118, 1716 – 1733, https://doi.org/doi:10.1002/jgrd.50203,
471 2013.
472 Singh, S., Kumar, R., Bhardwaj, A., Sam, L., Shekhar, M., Singh, A., Kumar, R., and Gupta, A.:
473 Changing climate and glacio-hydrology in Indian Himalayan Region: a review. Wiley
474 Interdisciplinary Reviews: Climate Change, 7, 393−410. https://doi.org/10.1002/wcc.393, 2016.
475 Singh, V. P., Sharma, N., and Ojha, C. S. P. (Eds.): The Brahmaputra Basin water resources, Kluwer
476 Academic Publishers, Dordrecht, Netherlands, 2004.
477 Teutschbein, C. and Seibert, J.: Bias correction of regional climate model simulations for
478 hydrological climate-change impact studies: Review and evaluation of different methods, Journal
479 of Hydrology, 456–457, 12–29, https://doi.org/10.1016/j.jhydrol.2012.05.052, 2012.
480 Wang, C., Ren, X., and Li, Y.: Analysis of extreme precipitation characteristics in low mountain
481 areas based on three-dimensional copulas—taking Kuandian County as an example, Theoretical and
482 Applied Climatology, 128, 169–179, https://doi.org/10.1007/s00704-015-1692-7, 2017.
483 Xu, R., Hu, H., Tian, F., Li, C., and Khan, M. Y. A.: Projected climate change impacts on future

484 streamflow of the Yarlung Tsangpo-Brahmaputra River, Global and Planetary Change, 175, 144–
485 159, https://doi.org/10.1016/j.gloplacha.2019.01.012, 2019.
486 Yatagai, A., Kamiguchi, K., Arakawa, O., Hamada, A., Yasutomi, N., and Kitoh, A.: APHRODITE:
487 Constructing a long-term daily gridded precipitation dataset for Asia based on a dense network of
488 rain gauges, Bulletin of the American Meteorological Society, 93, 1401−1415,
489 https://doi.org/10.1175/bams-d-11-00122.1, 2012.
490 Yucel, I. and Onen, A.: Evaluating a mesoscale atmosphere model and a satellite-based algorithm in
491 estimating extreme rainfall events in northwestern Turkey, Nat. Hazards Earth Syst. Sci., 14, 611–
492 624, https://doi.org/10.5194/nhess-14-611-2014, 2014.
493 Zhang Y., Zheng H., Herron N., Liu X., Wang Z., Chiew, F. H. S., and Parajka, J.: A framework
494 estimating cumulative impact of damming on downstream water availability, Journal of Hydrology,
495 575, 612–627, https://doi.org/10.1016/j.jhydrol.2019.05.061, 2019.
496

497 **Table 1.** Detailed description of extreme precipitation indices.

498

Table 1. Detailed description of extreme precipitation indices.

Index	Descriptive name	Definition	Unit
CWD	Consecutive wet days	Maximum number of consecutive days with precipitation ≥ 1 mm	days
R10mm	Number of heavy precipitation days	Count of days when precipitation ≥ 10 mm during June, July, August, and September (JJAS)	days
R20mm	Number of very heavy precipitation days	Count of days when precipitation ≥ 20 mm during JJAS	days
Rx1d	Maximum 1-day precipitation amount	Maximum 1-day precipitation	mm
Rx5d	Maximum 5-day precipitation amount	Maximum consecutive 5-day precipitation	mm
SDII	Simple daily intensity index	Total precipitation during JJAS divided by the number of wet days (when precipitation ≥ 1 mm)	mm/day

Figure 1. Locations of rainfall stations in the Yarlung Tsangpo-Brahmaputra River basin (YBRB).

Figure 2. Location of Asian Precipitation Highly Resolved Observational Data Integration Towards Evaluation of Water Resources (APHRODITE) grids over the Tibetan plateau (TP), Himalayan belt (HB), and floodplains (FP).

Figure 3. Mean error (*ME*) of (a) consecutive wet days (CWD), (b) number of heavy precipitation days (R10mm), (c) number of very heavy precipitation days (R20mm), (d) maximum 1-day precipitation amount (Rx1d), (e) maximum 5-day precipitation amount (Rx5d), and (f) simple daily intensity index (SDII) during June, July, August, and September (JJAS) for validation in the three different physiographic zones (TP, HB, and FP) of the YBRB.

Figure 4. Box-whisker plot for (a) CWD, (b) R10mm, (c) R20mm, (d) Rx1d, (e) Rx5d, and (f) SDII during JJAS in the three different physiographic zones (the TP, HB, and FP) of the YBRB derived from original and corrected APHRODITE estimates.

Figure 5. Relative change rate of (a) CWD, (b) R10mm, (c) R20mm, (d) Rx1d, (e) Rx5d, and (f) SDII during JJAS for original and corrected APHRODITE estimates.

Figure 6. Spatial distribution of mean Rx5d during JJAS in the YBRB based on (a) original APHRODITE estimates, as well as (b) linear scaling (LS)-APHRODITE estimates, (c) local intensity scaling (LOCI)-APHRODITE estimates, (d) power transformation (PT)-APHRODITE estimates, and (e) quantile−quantile mapping (QM)-APHRODITE estimates.

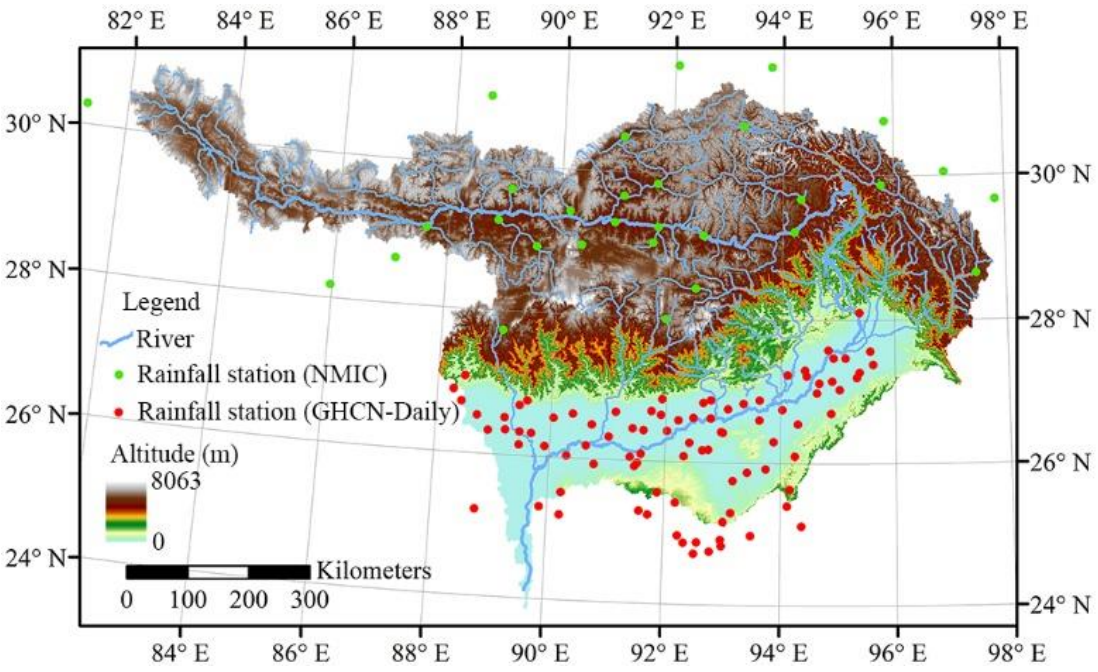

520

521 **Figure 1.** Locations of rainfall stations in the Yarlung Tsangpo-Brahmaputra River basin (YBRB).

522

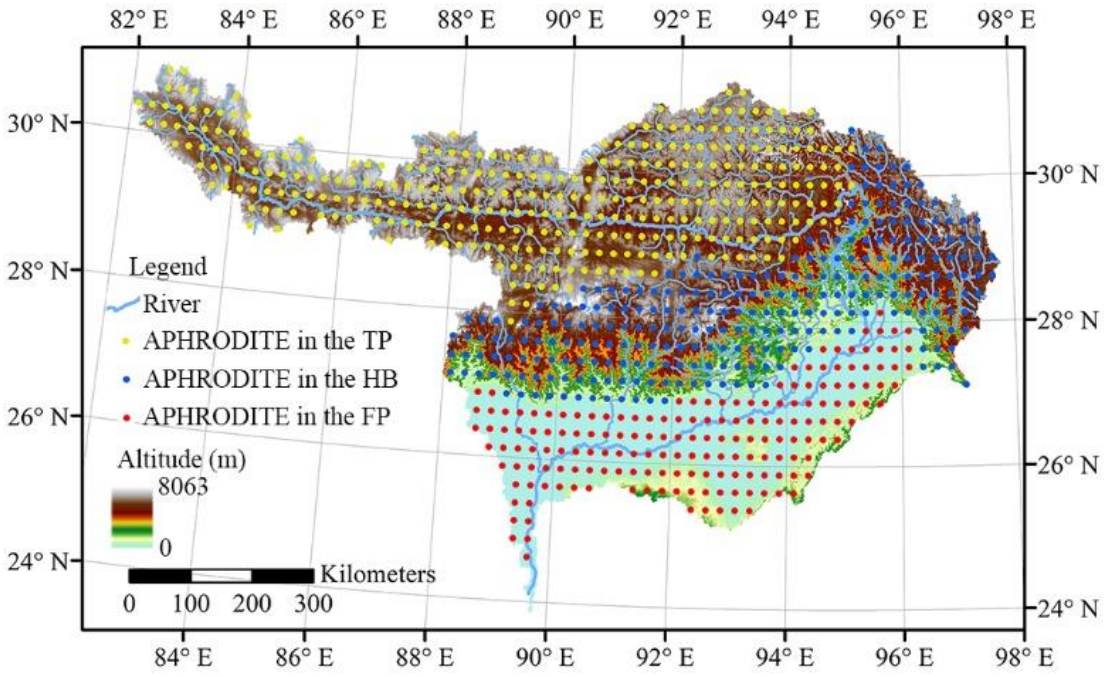

523

524 **Figure 2.** Location of Asian Precipitation Highly Resolved Observational Data Integration Towards

525 Evaluation of Water Resources (APHRODITE) grids over the Tibetan plateau (TP), Himalayan belt

526 (HB), and floodplains (FP).

527

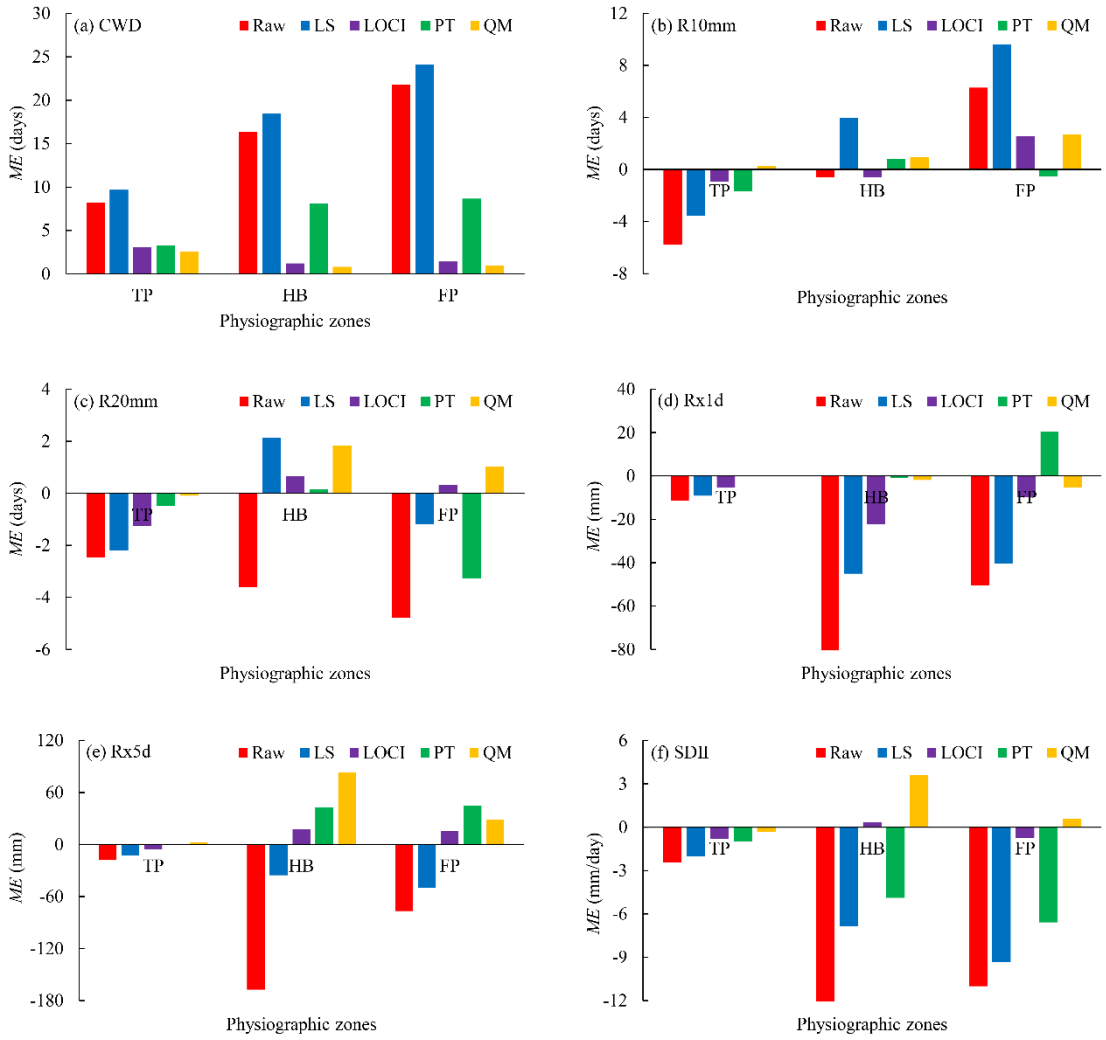

528

529 **Figure 3.** Mean error (*ME*) of (a) consecutive wet days (CWD), (b) number of heavy precipitation

530 days (R10mm), (c) number of very heavy precipitation days (R20mm), (d) maximum 1-day

531 precipitation amount (Rx1d), (e) maximum 5-day precipitation amount (Rx5d), and (f) simple

532 daily intensity index (SDII) during June, July, August, and September (JJAS) for validation in the

533 three different physiographic zones (TP, HB, and FP) of the YBRB.

534

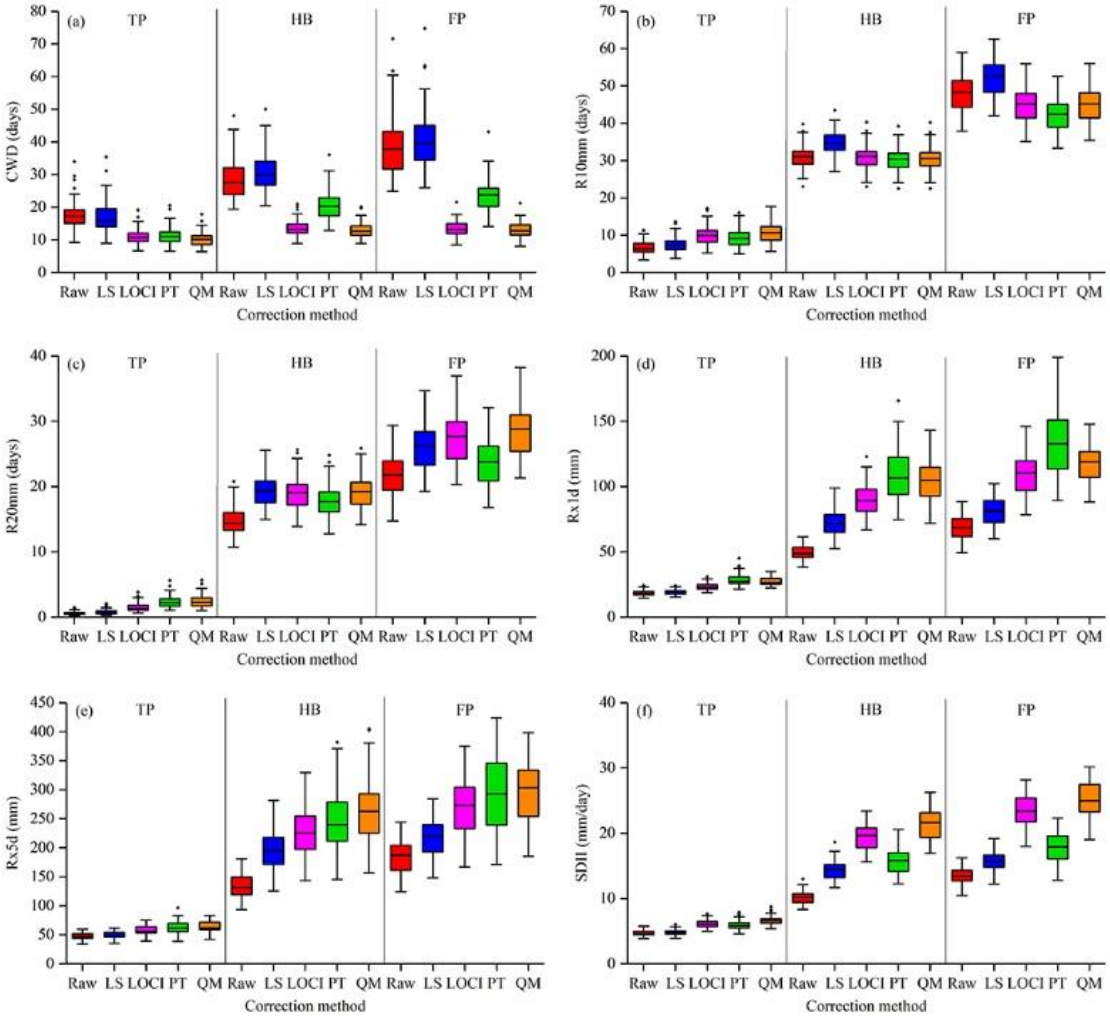

535

536 **Figure 4.** Box-whisker plot for (a) CWD, (b) R10mm, (c) R20mm, (d) Rx1d, (e) Rx5d, and (f) SDII

537 during JJAS in the three different physiographic zones (the TP, HB, and FP) of the YBRB derived

538 from original and corrected APHRODITE estimates.

539

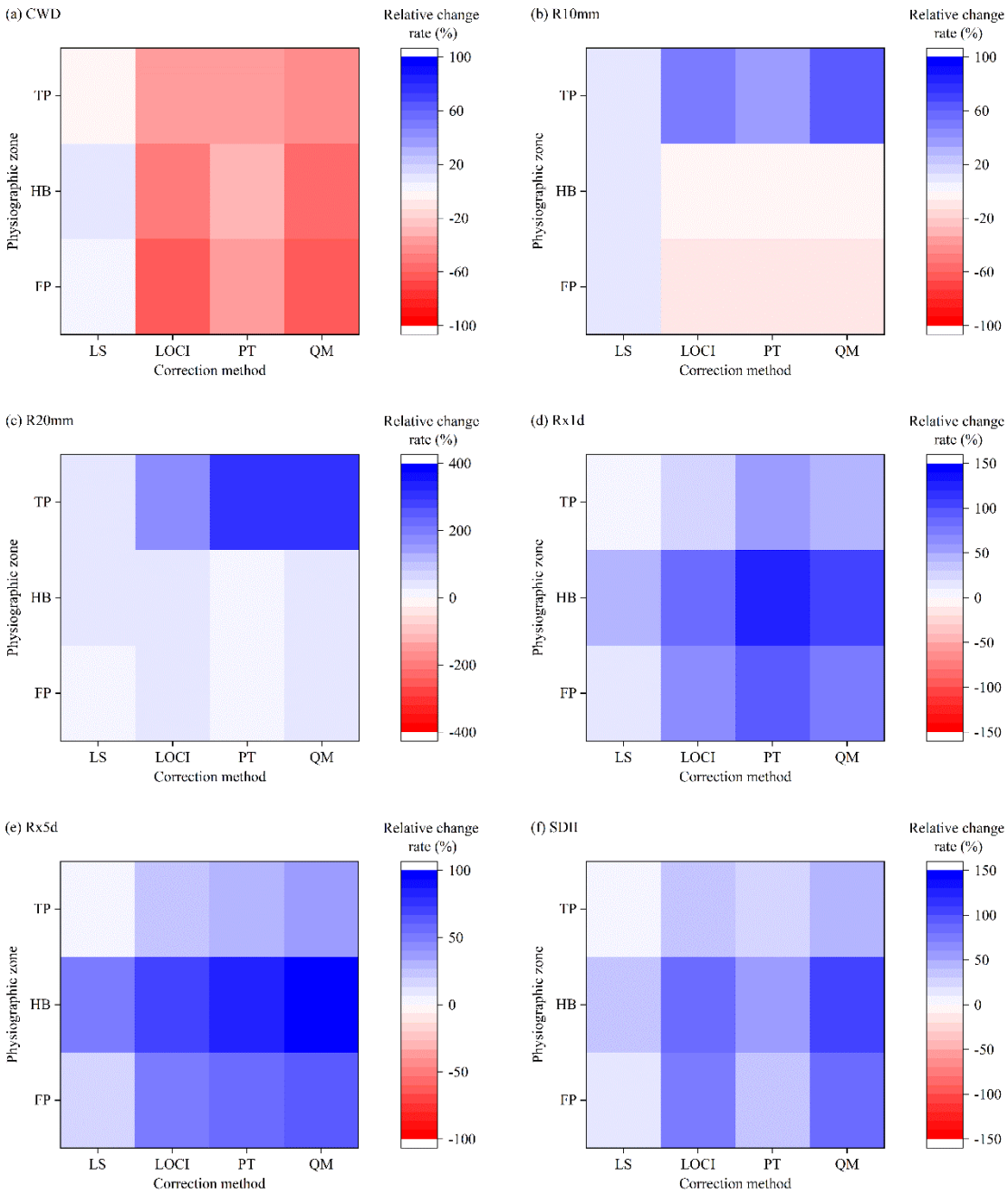

Figure 5. Relative change rate of (a) CWD, (b) R10mm, (c) R20mm, (d) Rx1d, (e) Rx5d, and (f) SDII during JJAS for original and corrected APHRODITE estimates.

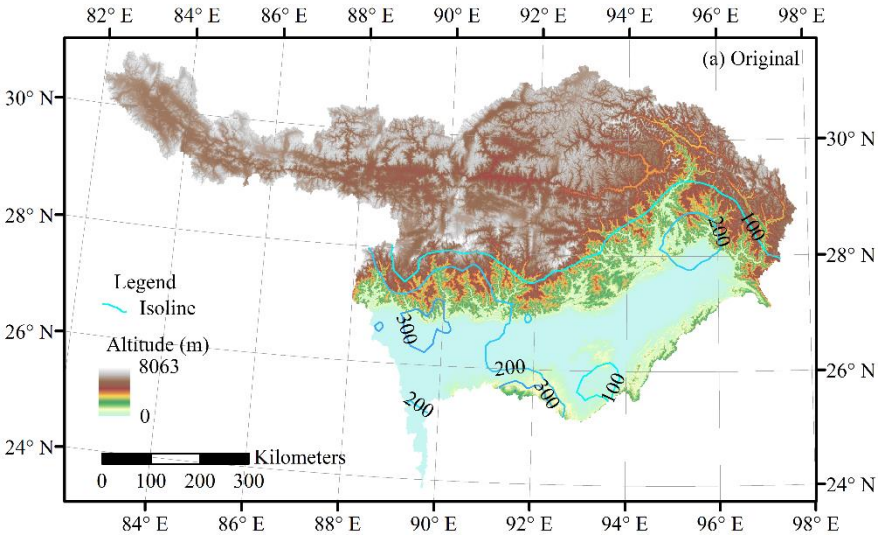
(a) Original
82° E
84° E
86° E
88° E
90° E
92° E
94° E
96° E
98° E
30° N
28° N
26° N
24° N
Legend
Isoline
Altitude (m)
8063
0
Kilometers
0 100 200 300

544

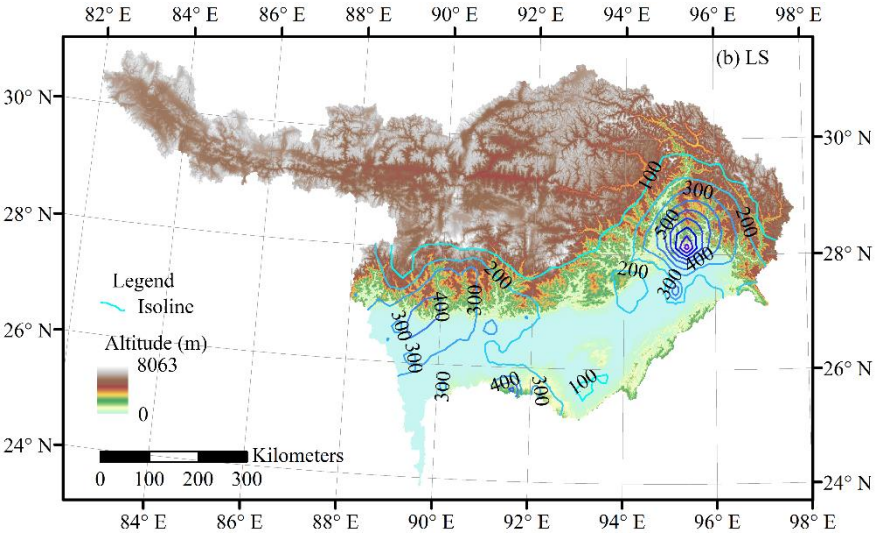
(b) LS
82° E
84° E
86° E
88° E
90° E
92° E
94° E
96° E
98° E
30° N
28° N
26° N
24° N
Legend
Isoline
Altitude (m)
8063
0
Kilometers
0 100 200 300

545

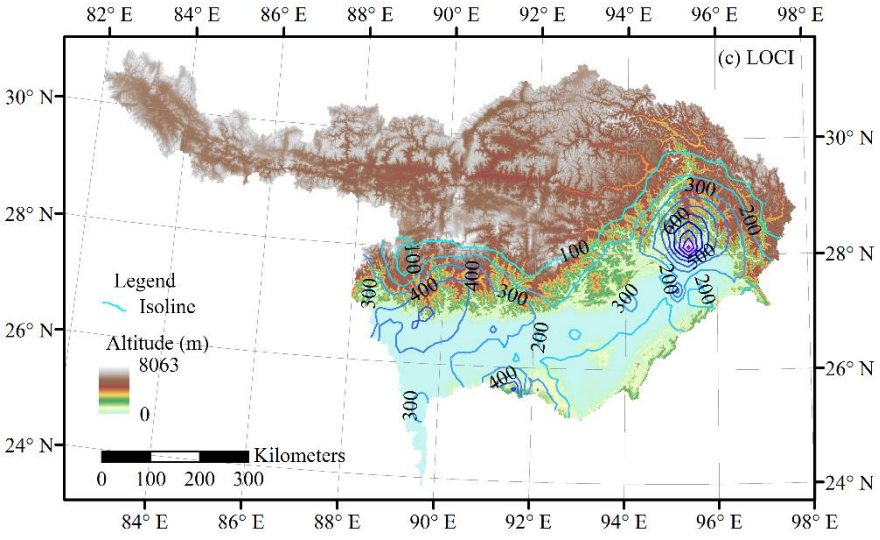
(c) LOCI
82° E
84° E
86° E
88° E
90° E
92° E
94° E
96° E
98° E
30° N
28° N
26° N
24° N
Legend
Isoline
Altitude (m)
8063
0
Kilometers
0 100 200 300

546

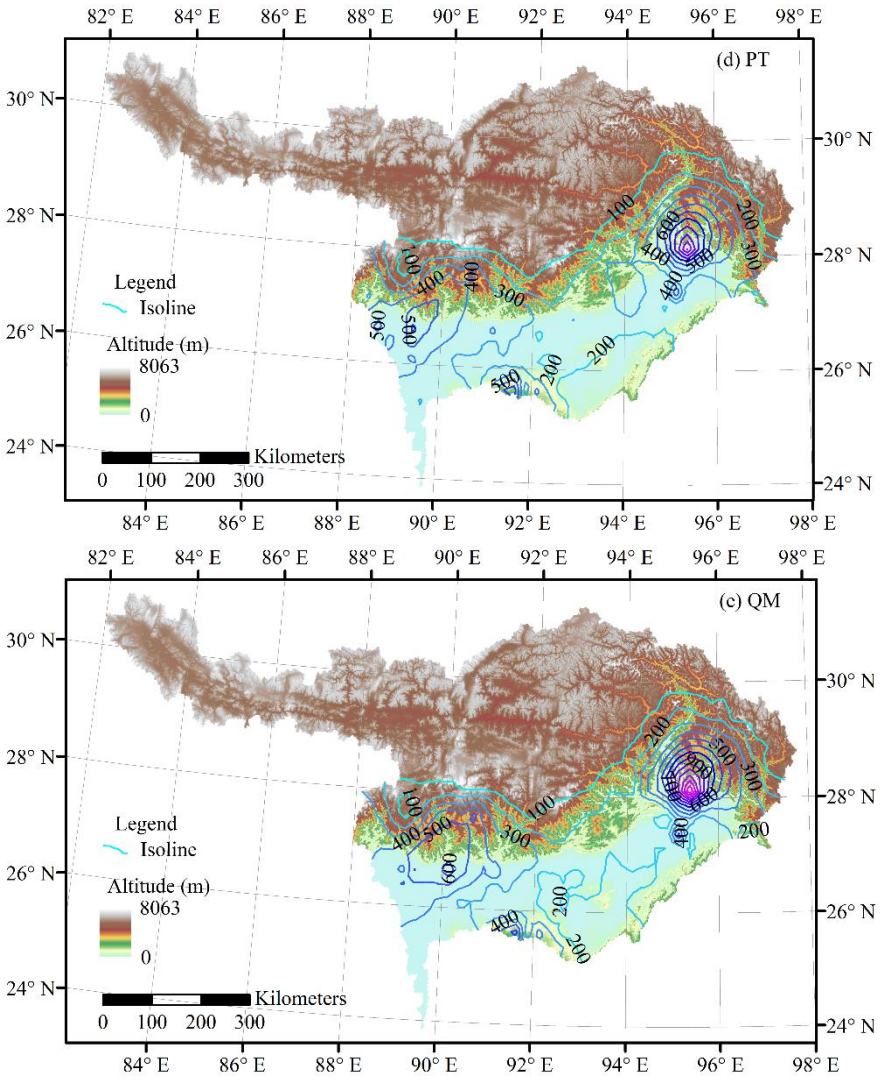

Figure 6. Spatial distribution of mean Rx5d during JJAS in the YBRB based on (a) original APHRODITE estimates, as well as (b) linear scaling (LS)-APHRODITE estimates, (c) local intensity scaling (LOCI)-APHRODITE estimates, (d) power transformation (PT)-APHRODITE estimates, and (e) quantile−quantile mapping (QM)-APHRODITE estimates.